# Experimental observation of the resonant doorways to the anion chemistry: the dynamic role of the dipole-bound Feshbach resonances in the dissociative electron attachment

Do Hyung Kang, Jinwoo Kim, Han Jun Eun and Sang Kyu Kim*

*Department of Chemistry, KAIST, Daejeon 34141, Republic of Korea*

*Corresponding Author: sangkyukim@kaist.ac.kr

## Abstract

Anion chemical dynamics of autodetachment and fragmentation mediated by the dipole-bound state (DBS) have been thoroughly investigated in a state-specific way for the first time by employing the picosecond time-resolved or the nanosecond frequency-resolved spectroscopy combined with the cryogenically cooled ion trap and velocity-map imaging techniques. For the *ortho*-, *meta*-, or *para*-iodophenoxide anion (*o*-, *m*-, or *p*-$IPhO^-$), the C-I bond rupture giving the anionic iodide ($I^-$) fragment occurs via the nonadiabatic transition from the DBS to the nearby valence-bound states (VBS) of the anion where the vibronic coupling into the $S_1$ ($\pi\sigma^*$) state (which is repulsive along the C-I bond extension coordinate) should be largely responsible. The dynamic details are governed by the isomer-specific nature of the potential energy surfaces in the vicinity of the DBS-VBS curve crossings, as manifested in the huge different chemical reactivity of *o*-, *m*-, or *p*-$IPhO^-$. It is confirmed here that the C-I bond dissociation is mediated by DBS resonances, providing the foremost evidence that the metastable DBS plays the essential role as the doorway into the anion chemistry especially of the dissociative electron attachment (DEA). The fragmentation channel is dominant when it is mediated by the DBS resonances located below the electron-affinity (EA) threshold, whereas it is kinetically adjusted by the competitive autodetachment process when the DBS resonances lying above EA convey the electron to the valence orbitals. The product yield of the C-I bond cleavage is strongly mode-dependent as the rate of the concomitant autodetachment is much influenced by the characteristics of the individual vibrational modes, paving a new way of the reaction control of the anion chemistry.

Since it was firstly conceived by Fermi and Teller in 1947,[1] the dipole-bound state (DBS) of the anion has been both extensively and intensively investigated for many recent decades in terms of its structure and dynamic role[2-5] as its study becomes increasingly important for understanding the whole anion chemistry and physics in many aspects.[6-8] The lower limit of the dipole moment for the DBS formation had been initially predicted to be 1.627 D, although it seems to be now widely regarded (as a rule of thumb) that the excess electron could be attached to the neutral core when its dipole moment exceeds ~ 2.5 D.[9-11] It should be emphasized though that the nature of the binding force between the excess electron and neutral core seems to be not straightforward as much as the literal meaning of the DBS may imply. Namely, the interaction potential is rather complex as all the possible monopole-multipole (such as dipole or quadruple) interactions as well as the correlation effect should contribute corroboratively to the binding dynamics of the excess electron to the neutral core though the extents of their contributions should vary depending on the particular chemical systems under various circumstances.[12, 13] In this regard, it may be fair to state that the DBS belongs to the category of the non-valence bound state (NBS) in a sense that its excess electron does not occupy any empty valence orbital whereas the more stable anion of which the excess electron resides in the valence orbital could be called the valence bound state (VBS).

DBS has been ubiquitously found in a variety of chemical or biological systems, ranging from small organic to large biological molecules or clusters.[14-21] Recent spectroscopic studies have suggested that the DBS could be a primary candidate for the carrier of the diffuse interstellar species and/or the interstellar PAH anions, giving the enormous astrochemical implication.[22-25] The anion chemistry/physics provoked by the electron-attachment is ubiquitously found not only in the atmospheric or interstellar species but also in a variety of biological/chemical processes such as photosynthesis,[26] destruction/relaxation of DNA bases,[27-29] or signaling of the fluorescent proteins.[30] As the size of the dipole-bound orbital is almost identical to the de Broglie wavelength of the incoming electron, the electron attachment to the neutral in the frame of DBS is extremely efficient.[16, 31] In this aspect, it should be noted that the DBS has also long been conceived as the

major doorway in the dissociative electron attachment (DEA) process where the slow electron is captured to be followed by the immediate rupture of the specific chemical bond.[32-35] DEA is ubiquitously found, ranging from chemistry of the small environmentally important oxide species to radiative damages of biological genetic species such as DNA/RNA double/single helices.[36-39] Although the DEA dynamics have been much investigated in some elegant experiments,[40-44] the rather direct experimental evidence for the role of the DBS in the DEA has been quite rare to date. The anionic DBS either loses the excess electron by the autodetachment process or undergoes the transformation into the more stable valence bound anion via the radiative and/or nonradiative transitions before it may be followed by the subsequent chemical reactions. Despite that the autodetachment dynamics of DBS has been quite intensively and extensively investigated for recent years,[5, 45] the structural dynamics involved in the anion formation at various electronic states and its associated chemistry/physics especially mediated by the quantum resonant states of the DBS (as the doorways) have been far from the complete understanding.

Recent real-time pump-probe experimental studies on the state-specific dynamics of the cryogenically-cooled anions such as phenoxide and some of its analogues have revealed that the dynamic range of the DBS is quite wide especially in terms of its mode-specific lifetime.[46-48] For the phenoxide anion, for instance, the DBS prepared below the photodetachment threshold decays quite slowly with its lifetime longer than tens of nanoseconds whereas the vibrational autodetachment of DBS above the detachment threshold takes place quite rapidly with a typical lifetime of tens of picoseconds. This experimental fact suggests that the DBS may undergo the rather slow radiative or nonradiative transition to the ground or excited state of the anion when the total energy is below the electron detachment threshold. On the other hand, when the internal energy given to the DBS gets higher than the detachment threshold, the excess electron is liberated very rapidly by the strong coupling between the electronic and nuclear motions. Actually, it has been found that the Fermi's golden rule for such a coupling is extremely useful in accounting for the mode-specific autodetachment rates of the phenoxide,[47] although the intrinsic

complicated nature of the binding dynamics of the DBS requires the more sophisticated theoretical models which are needed to be adapted for different chemical systems. The obvious question thereafter is related to the nature of the DBS relaxation process. Does it really play the role as a doorway in its transformation into the ground (or excited) state of the valence-bound anion? If so, what would be the overall mechanism of the DBS–VBS transition in terms of the dynamic and kinetic properties?

Herein, we have investigated the autodetachment and fragmentation dynamics of *ortho*-, *meta*-, and *para*-iodophenoxide (*o*-, *m*-, and *p*-$IPhO^-$) anions. Vibrational Feshbach resonances of the DBS have been found for all three cryogenically-cooled anions although their dynamics are found to be quite distinct in terms of the state-specific lifetimes and associated chemistries. Especially, the competitive dynamics among the autodetachment and nonadiabatic transitions have been thoroughly investigated in a state-specific way by employing the picosecond time-resolved or the nanosecond frequency-resolved spectroscopy combined with the cryogenically cooled ion trap and the velocity-map electron imaging techniques.[49, 50] Nonadiabatic couplings through the curve crossings of the potential energy surfaces of the DBS and those of the nearby anionic valence electronic states govern the anion formation dynamics at particular electronic state(s) and subsequent chemical reactions, reflecting the quantum-mechanical dynamic role of the DBS as the doorway into the anion chemistry. Quite interestingly, the C-I chemical bond rupture (giving the $I^-$ fragment) occurs near the photodetachment threshold for all three anions with the strong mode specificity, giving the unprecedented insights into the coupling between nuclear and electronic motions along the passages connecting the DBS and VBS in terms of the electron-attachment/detachment physics and fragmentation chemistry. This report provides one of the foremost experimental evidences for the actual dynamic role of the DBS as the doorway to the anion physics and chemistry.

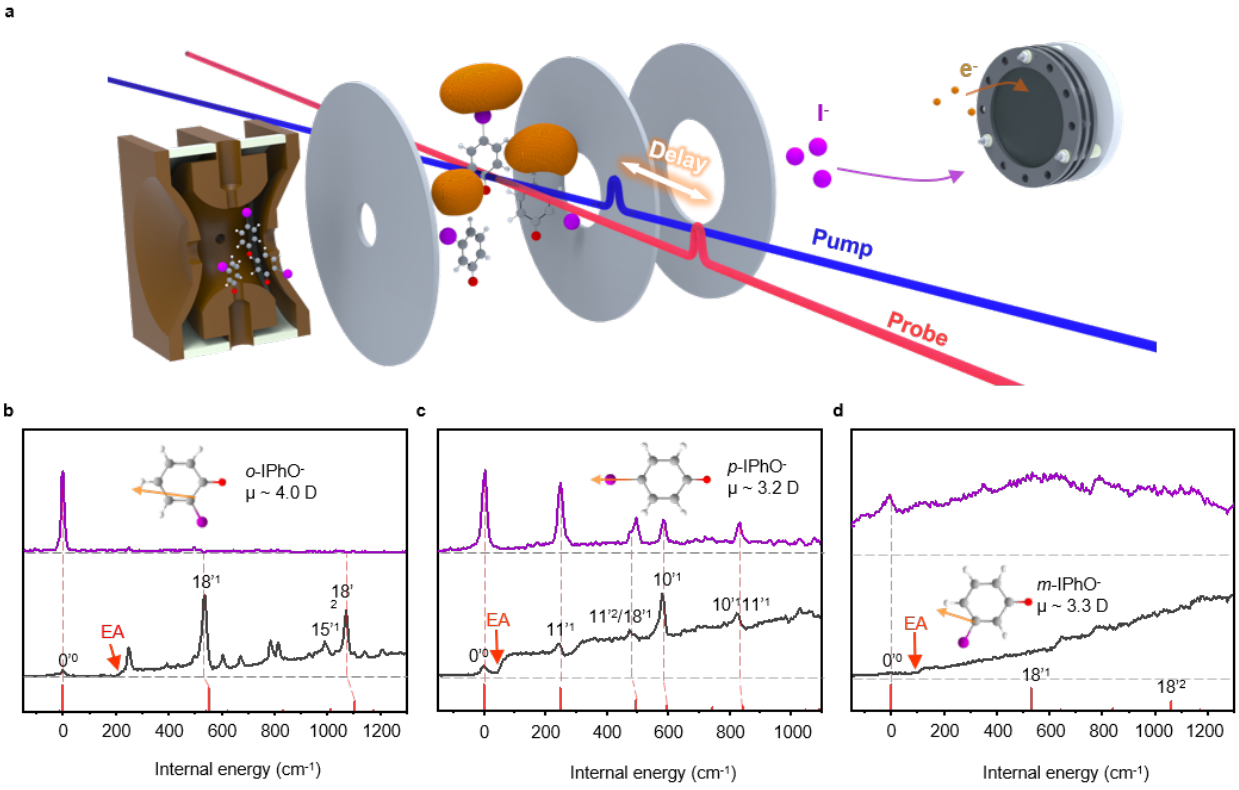


**Fig. 1 Photodetachment ($e^-$) and the $I^-$ fragment action spectra of *ortho-*, *meta-*, or *para*-iodophenoxide anions.** **a** Sketch of the experiment for the photofragment or photodetachment spectrum of *o*-, *m*-, and *p*-$IPhO^-$. The frequency-resolved nanosecond or the time-resolved picosecond (pump-probe) spectroscopy has been carried out to detect the photoelectron or the $I^-$ fragment. The resultant photodetachment spectra (black) and the $I^-$ fragment action spectra (violet) of **b** *o*-$IPhO^-$, **c** *p*-$IPhO^-$ and **d** *m*-$IPhO^-$ are shown with the Franck-Condon (FC) simulations for the vertical $S_0$-$D_0$ transitions (red sticks). The EA threshold and the DBS vibrational modes of each anion are denoted. Grey dotted horizontal lines represent the zero-baselines in the absence of the laser-ion interaction. The optimized geometries of the neutral ground state and its dipole moment are depicted in insets.

Non-resonant photoelectron spectra of the cryogenically-cooled anions of *o*-, *m*-, and *p*-$IPhO^-$ give the precise electron affinities (EAs) and structural changes upon the photodetachment, from their lowest electron binding energies and the Franck-Condon active vibrational modes, respectively (see Supplementary Fig. S1). Overall, the in-plane stretching mode along the C-O bond axis ($\nu_{18}$ or $\nu_{11}$) is found to be highly activated, reflecting the structural changes of the iodophenoxide anions upon the instantaneous photodetachment process. The EA of each anion has been refined by the extrapolation method from a series of photoelectron spectra obtained at

many different photon energies (Supplementary Fig. S2), giving the EA value of 21,656 ± 13, 21,778 ± 24, or 21,051 ± 15 $cm^{-1}$ for *o*-$IPhO^-$, *m*-$IPhO^-$, or *p*-$IPhO^-$, respectively. The EA of *p*-$IPhO^-$ is in good agreement with the previous one of 21,046 $cm^{-1}$ reported from the Wang group.[10] Notably, EA of *m*-$IPhO^-$ is larger than that of *o*-$IPhO^-$ or *p*-$IPhO^-$. This could be attributed to the destabilization of the latter anions (*o*-$IPhO^-$ and *p*-$IPhO^-$) by the π-orbital donation to the benzyl ring of specific resonance forms. The larger EA value of *o*-$IPhO^-$ compared to that of *p*-$IPhO^-$ could be due to the relatively stronger inductive effect of the electronegative iodine atom in the former than that in the latter. These trends had been repetitively found in other different halogen-substituted benzyl[51] or methyl-substituted phenoxyl anions.[52, 53]

Now, the photodetachment spectra of *o*-, *m*-, and *p*-$IPhO^-$ taken by monitoring the total photoelectron yield as a function of the excitation (pump) photon energy using the nanosecond laser pulse ($\Delta E$ ~ 3.5 $cm^{-1}$, $\Delta t$ ~ 4.2 ns) give rise to metastable vibrational Feshbach resonance states of DBS as sharp peaks in addition to the broad background signal arising from the direct electron detachment, Fig. 1. Obviously, a number of vibrational Feshbach resonances are well pronounced in *o*- and *p*-$IPhO^-$ whereas the identification of those seems to be less straightforward in *m*-$IPhO^-$ (*vide infra*). The photodetachment spectrum of *o*-$IPhO^-$ shows the DBS resonances strongly enhanced especially at the fundamental and overtone of the in-plane ring stretching ($\nu_{18}$) mode at the internal energy ($E_{int}$) of ~ 532 and ~ 1070 $cm^{-1}$, respectively, indicating that the geometry of DBS remains unaltered from that of the neutral radical as expected. The zero-point level (ZPL) is clearly identified as a peak located just below the EA threshold, giving the electron binding energy (eBE) of ~ 231 $cm^{-1}$ for the DBS of *o*-$IPhO^-$. The photodetachment spectrum of *p*-$IPhO^-$ also gives the distinct vibrational Feshbach resonances above the featureless direct background signal although those are relatively less pronounced compared to the case of *o*-$IPhO^-$. The DBS resonances of the $\nu_{11}$ ($E_{int}$ ~ 245 $cm^{-1}$) and $\nu_{10}$ ($E_{int}$ ~ 580$cm^{-1}$) modes as well as their overtone or combination bands are clearly identified for *p*-$IPhO^-$. It is a bit surprising that the DBS bands are nearly absent in the photodetachment spectrum of *m*-$IPhO^-$ despite that the dipole moment of its neutral radical is large enough (3.30 Debye) to hold an excess electron. The stepwise increases at

the threshold and 530 $cm^{-1}$ above EA should be ascribed to the cumulative openings of the direct detachment channels according to the Franck-Condon factor. The ZPL just below the EA threshold is barely identified to give the eBE of ~ 97 $cm^{-1}$ for the DBS of *m*-$IPhO^-$ (*vide infra*). The photodetachment spectra have also been obtained by using the picosecond laser pulse ($\Delta E$ ~ 20 $cm^{-1}$), giving the slightly less distinct spectral features though the overall features remain unchanged for all three anions (Supplementary Information). Photoelectron spectra taken at the vibrational Feshbach resonances reveal the clear-cut autodetachment feature of $\Delta v = -1$ (obeying the propensity rule)[54-56] for *o*-$IPhO^-$ and *p*-$IPhO^-$, whereas we could hardly detect the auto-detached photoelectron in the photoelectron images for *m*-$IPhO^-$.

The real-time dynamics of vibrational Feshbach resonances, taken from the pump-probe time-resolved photoelectron images (TR-PEI), provide the lifetimes of individual DBS vibrational states in a state-specific way. The picosecond excitation laser pulse (pump) populates the specific DBS resonant state whereas the 791 nm picosecond laser pulse (probe) depopulates the initial state into the detachment continuum to give the high kinetic energy electron (Fig. 2**a**). The photoelectron yield in the low or high kinetic energy region is then separately monitored as a function of the delay time between pump and probe pulses. The typical photoelectron transient monitoring the low kinetic energy exhibits the initial depletion at the zero time-delay followed by the immediate recovery apparently at the rate of the autodetachment process. The high kinetic energy photoelectron transient, on the other hand, reflects the rather direct real-time decay of the DBS population. For *o*-$IPhO^-$, the low kinetic energy photoelectron transient of the most prominent $18'^1$ band (532 $cm^{-1}$) gives the autodetachment lifetime ($\tau$) of 12.3 ± 2.2 ps whereas that of the $15'^1$ band (989 $cm^{-1}$) gives $\tau$ ~ 4.0 ± 0.9 ps (Fig. 2). Within the experimental uncertainties, these are quite consistent with the DBS lifetime of 10.1 ± 0.8 or 6.3 ± 0.7 ps obtained from the high kinetic energy transient of the $18'^1$ or $15'^1$ mode, respectively. Lifetimes of the DBS modes of *p*-$IPhO^-$ taken from the high-kinetic energy transients are found to be much shorter, giving $\tau$ ~ 3.4 ± 1.2 or 4.5 ± 1.3 ps for the $11'^1$ or $10'^1$ mode, respectively. For the $11'^1$ mode of *p*-$IPhO^-$, it is quite notable that the signal of the low kinetic energy photoelectron arising from the autodetachment

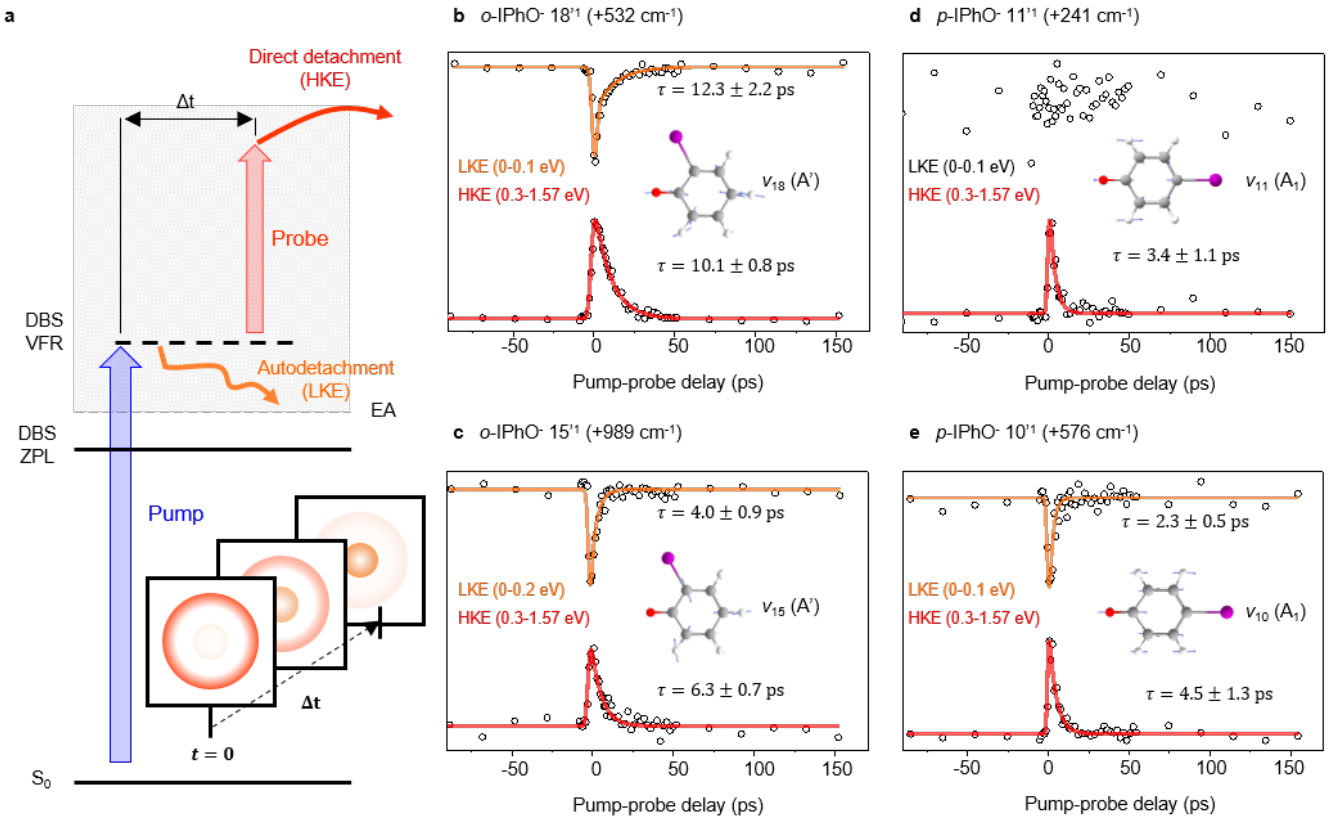


**Fig. 2 Picosecond time-resolved photoelectron transients of *o*-IPhO⁻ or *p*-IPhO⁻ at specific vibrational Feshbach resonances of the DBS. a** Schematic diagram of the picosecond time-resolved photoelectron imaging (TR-PEI) obtained at vibrational Feshbach resonances (VFR) of the DBS. Picosecond pump laser pulse populates specific vibrational states of the DBS and then the temporally-delayed probe laser pulse depopulates into the detachment continuum yielding the high kinetic energy electron (HKE). The temporal evolution of the electron originating from autodetachment is revealed in the low-kinetic energy (LKE) region (orange) whereas that of the DBS population is reflected in the HKE (red), giving the transients of the **b** $18'^1$ and **c** $15'^1$ modes of *o*-IPhO⁻. For *p*-IPhO⁻, transients of the **d** $11'^1$ and **e** $10'^1$ modes are shown. Photoelectron transients in LKE region (0-0.1 or 0-0.2 eV, orange) are in good agreement with those in HKE region (0.3-1.57 eV, red). For the $11'^1$ mode of *p*-IPhO⁻, the LKE transient is hardly discernable due to the very low autodetachment yield (see the text). Normal mode of each vibrational band is depicted in insets. Each transient was fitted by the single exponential decay function convoluted with the instrumental cross-correlation function.

is extremely weak, hampering to obtain the corresponding transient with the decent signal to noise ratio (*vide infra*). It is also quite noteworthy that the lifetime of the DBS band of *p*-IPhO⁻, unlikely from that of *o*-IPhO⁻, is little mode-dependent even though the autodetachment rate is expected to be strongly influenced by the infrared (IR) intensity of the particular vibrational mode

according to the Fermi's golden rule.[47, 57-59] For instance, the IR intensity of the $10'^1$ mode is calculated to be ~ 120 times stronger than that of the $11'^1$ mode of *p*-IPhO$^-$ (Supplementary Information). Surprisingly, however, the DBS lifetimes of the $10'^1$ and $11'^1$ modes are found to be more or less same. This experimental finding strongly indicates that the autodetachment may not be the major relaxation pathway of the DBS for *p*-IPhO$^-$. Actually, in our previous report, the lifetime of the DBS at ZPL below the EA threshold has been found to be exceptionally short to give $\tau \sim 9$ ps for *p*-IPhO$^-$.[46] As the autodetachment is intrinsically blocked at ZPL, the short lifetime has been attributed to the fast internal conversion to the low-lying $S_1$ state ($\pi\sigma^*$) which is repulsive along the C-I bond elongation coordinate, eventually leading to the $\cdot C_6H_4O\cdot$ radical and $I^-$ fragments at the asymptotic limit. It is therefore highly anticipated that such a fast internal conversion of the DBS into the anionic excited state ($S_1$) persists also at Feshbach resonances above the EA threshold, resulting in their even shorter and little mode-dependent lifetimes as well as the relatively small yields of the auto-detached photoelectron (*vide infra*).

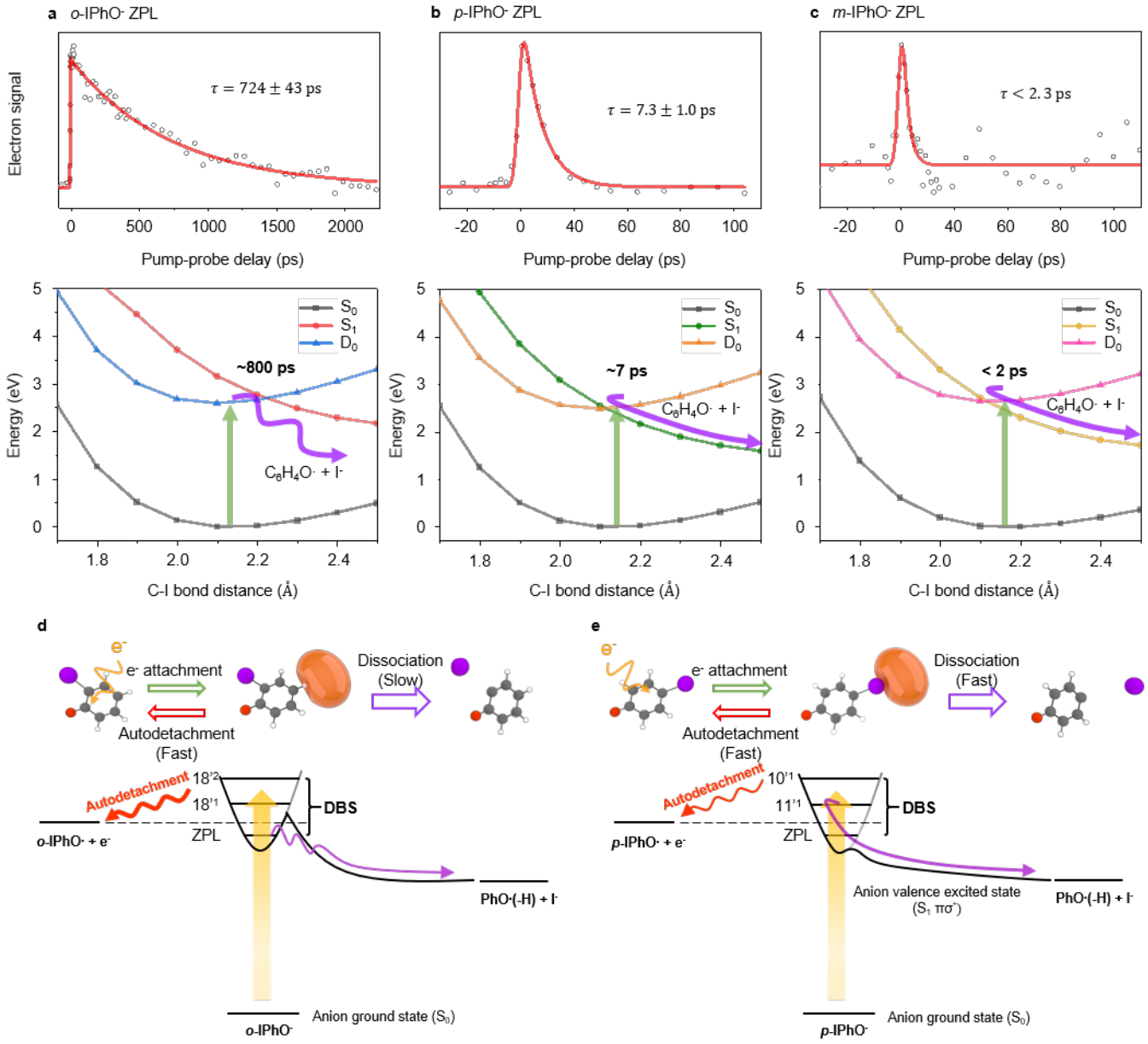


**Fig. 3 Non-adiabatic relaxation pathways from the ZPLs of DBSs into the nearby $S_1$ ($\pi\sigma^*$) valence excited anionic states eventually leading to the production of the $I^-$ fragment.** (Upper trace) The picosecond time-resolved photoelectron transient of **a** *o*-IPhO$^-$, **b** *p*-IPhO$^-$, or **c** *m*-IPhO$^-$ obtained at the ZPL of DBS with the fit using the single-exponential decay function (see the Fig. 2 caption). (Middle trace) Potential energy curves of $S_0$ (anion ground state), $S_1$ ($\pi\sigma^*$), and $D_0$ (neutral ground state) states along the C-I bond elongation coordinate calculated by the B3LYP/Def2tzvp level of theory with Gaussian 09 packages (see the text). (Lower trace) Schematic diagram of the competition dynamics of DEA from the DBS of **d** *o*-IPhO$^-$ or **e** *p*-IPhO$^-$.

The more systematic approach has been made for the comparison of three different anions in terms of their behaviors at ZPLs located just below their EA thresholds where the autodetachment is intrinsically blocked. The TR-PEI transient obtained at ZPL of the *o*-IPhO$^-$ DBS gives the relatively long lifetime of 724 ± 43 ps (Fig. 3), suggesting that the internal conversion and/or intersystem crossing (ISC) into the low-lying anionic states should have been significantly slowed down. This indicates that the rather fast direct relaxation into the repulsive σ* state of the anion is not likely to be engaged in the DBS dynamics at the ZPL of *o*-IPhO$^-$. The lifetime obtained from TR-PEI for the ZPL of the *p*-IPhO$^-$ DBS, on the other hand, is estimated to be 7.3 ± 1.0 ps, indicating that the fast internal conversion to the low-lying $S_1$ state ($\pi\sigma^*$) is engaged in this rather unusual short lifetime. More dramatically, the relaxation of the *m*-IPhO$^-$ DBS at ZPL is found to be extremely fast to give $\tau$ < ~ 2 ps, which is beyond the limit of the current instrumental response function (IRF) of ~ 2.8 ps. This strongly indicates that the nearby anionic states are strongly coupled to DBS even at the ZPL. The apparent absence of the DBS resonant features in the photodetachment spectrum of *m*-IPhO$^-$ (Fig. 1) thus could be readily rationalized by the fact that the autodetachment process of *m*-IPhO$^-$ (which is totally responsible for the photoelectron signal originating from the DBS resonances) should be diminished as the DBS relaxation pathway is overwhelmed by the much faster nonradiative transition to the short-lived anionic valance state(s).

In order to invoke the possible relaxation mechanism therein, the time-dependent density functional theory (TD-DFT) has been employed for calculating the low-lying valence electronic states of anions. As previously reported for *p*-IPhO$^-$,[46] the first electronically-excited singlet state ($S_1$) is predicted to be closely located to the EA threshold for all three iodine-substituted phenoxide anions. For all of *o*-, *m*-, and *p*-IPhO$^-$, the $S_1$ ($\pi\sigma^*$) is found to be repulsive in nature along the C-I bond extension coordinate leading to the ultrafast C-I bond rupture to give the I$^-$ fragment at the asymptotic limit; it should be noted that only the I$^-$ fragment channel (which is diabatically correlated to $S_1$) is thermodynamically plausible (see Supplementary Materials). The

energetic location of the anionic $S_1$ state with respect to the neutral ground state ($D_0$) is quite different for the chemical species of three different substitution positions. Interestingly, the anionic $S_1$ state is predicted to be located below the EA threshold for *p*-$IPhO^-$ or *m*-$IPhO^-$, whereas that of *o*-$IPhO^-$ lies above the EA threshold (Fig. 3). The vertical energy gap between $S_1$ and $D_0$ at the minimum energy structure of the ground anionic state is calculated to be ~ 0.08 or ~ 0.21 eV for *p*-$IPhO^-$ or *m*-$IPhO^-$, respectively, indicating that the corresponding DBSs are expected to be quite vulnerable to the rapid internal conversion processes into the low-lying repulsive $S_1$ states of VBSs. This strongly supports the experimental results that DBS lifetimes are exceptionally short (even at ZPL) for both *p*-$IPhO^-$ and *m*-$IPhO^-$, and they are little influenced by the mode characteristics. It is quite notable that the $S_1$-$D_0$ gap of *m*-$IPhO^-$ is predicted to be much larger than that of *p*-$IPhO^-$, and this might be the reason for the earlier dominance of the DBS-VBS ($S_1$) transition in the ultrafast relaxation of the former compared to the case of the latter (*vide infra*). The dominance of the ultrafast internal conversion should be then responsible for the featureless photodetachment spectrum of *m*-$IPhO^-$ (Fig. 1) as the competitive but relatively slower autodetachment channel is diminished even for the vibrational Feshbach resonances above the EA threshold. On the contrary, $S_1$ is calculated to be located much higher than $D_0$ for *o*-$IPhO^-$, giving the vertical gap of ~ 0.41 eV between $S_1$ and $D_0$. Thereby, the transformation from the DBS into the short-lived VBS ($S_1$) is expected to be much less facilitated in *o*-$IPhO^-$, perfectly explaining its much longer lifetime of the DBS at the ZPL (Fig. 3). As the excitation energy increases, the relatively faster autodetachment process becomes dominant at the DBS Feshbach resonances above EA compared to the (rather slow) nonradiative transition into anionic state(s), giving the much-pronounced DBS bands in the photodetachment spectrum of *o*-$IPhO^-$ (Fig. 1).

Although the energetic hierarchy among electronic states at various configurations should be one of the important factors in determining destinations of the relaxation pathways, the nonadiabatic transitions are particularly anticipated to be facilitated at the curve crossing region. As we are dealing with the chemical reaction of the C-I bond rupture, the potential energy curves of the low-lying electronic states of anions ($S_0$ and $S_1$) as well as the potential surface of the

neutral ($D_0$) are calculated along the C-I bond extension coordinate. It should be emphasized that the overall shape of the potential energy surface of the DBS should be little different from that of the neutral radical ($D_0$). Being consistent with the experiment, the curve-crossing region of $D_0$ and $S_1$ is calculated to be located quite close to the vertical excitation window between the anionic ground state ($S_0$) and DBS as long as the one-dimensional C-I bond extension coordinate is concerned for both *m*-$IPhO^-$ and *p*-$IPhO^-$ (Fig. 3). This strongly supports the ultrafast nonadiabatic DBS-VBS ($S_1$) transition. On the other hand, the $D_0$-$S_1$ curve crossing point of *o*-$IPhO^-$ is predicted to be quite remote from the vertical excitation window, suggesting that the substantial structural change (at least along the C-I bond extension coordinate) is required for the nonadiabatic transition to be efficiently activated. This may explain why the DBS lifetime of *o*-$IPhO^-$ at the ZPL is significantly longer than that of *m*-$IPhO^-$ or *p*-$IPhO^-$. This also provide the reason why DBS resonant bands above EA are quite pronounced only in the photodetachment spectrum of *o*-$IPhO^-$, as their relaxation pathways are dominated by the much faster autodetachment processes (*vide supra*), differently from the case of *m*-$IPhO^-$ or *p*-$IPhO^-$.

Probing the final destination of the DBS-mediated anionic excited states would be the smoking gun for the whole anion physics/chemistry presented here. We could successfully probe the $I^-$ fragment in the current experimental setup. By employing the intense and tunable nanosecond laser pulse, the product action spectra have been obtained by monitoring the $I^-$ fragment yield as a function of the excitation energy for all three anions, Fig. 1. The $I^-$ fragment yield is strongly and resonantly enhanced quite significantly at the ZPL of the DBS for *o*-$IPhO^-$, whereas it is substantially decreased to be barely observable at all additional DBS resonances lying above the EA threshold. This strongly indicates that the fragmentation resulting from the DBS-VBS transition occurs predominantly only when the autodetachment process is intrinsically blocked. The relatively faster autodetachment process then becomes the dominant relaxation pathway at the DBS vibrational Feshbach resonances above EA, and the relatively slower DBS-VBS transition pathway of *o*-$IPhO^-$ is much suppressed. While the ultrashort lifetime of the DBS found at the ZPL of *m*- or *p*-$IPhO^-$ strongly indicates that the nonadiabatic DBS-VBS ($S_1$) transition

is quite rapid and responsible for the $I^-$ fragment, the destination of the DBS-VBS transition in terms of the nature of the anionic electronic state(s) involved does not seem to be conclusive yet for the case of *o*-$IPhO^-$. Namely, quite differently from the case of *m*- or *p*-$IPhO^-$, the repulsive $S_1$ state is predicted to be located much above $D_0$ for *o*-$IPhO^-$ in the vertical transition region. The DBS flux at the ZPL then has to overcome the barrier of ~ 1300 $cm^{-1}$ at least along the C-I bond extension coordinate for its transformation into the repulsive $S_1$ state of VBS. The DBS lifetime of ~ 724 ps measured at the ZPL of *o*-$IPhO^-$ (Fig. 3) may thus reflect the rather slow DBS-VBS ($S_1$) transition taking place with the significantly large barrier, although the multi-dimensional potential energy surfaces are required for grasping the nuclear configurations in the curve-crossing region. The other pathway of the DBS-VBS transition into $S_0$ (internal conversion) or $T_1$ (intersystem crossing) which could also lead to the eventual C-I bond cleavage cannot be excluded at the present time. The angular and kinetic analyses of the $I^-$ fragment would be extremely helpful for the more complete description of the relaxation mechanism of *o*-$IPhO^-$.

The more remarkable feature could be found in the fragment-action spectrum of *p*-$IPhO^-$. Here, the $I^-$ fragment yield is strongly enhanced for all DBS resonant bands regardless their positions with respect to the EA threshold, Fig. 1, indicating that the autodetachment (responsible for the resonant photoelectron signal in the photodetachment spectrum) and the DBS-VBS transition (responsible for the $I^-$ fragment yield) concomitantly occur quite competitively even when the former channel is fully opened as the latter process is also quite rapid for *p*-$IPhO^-$. The relative yields of the DBS-resonant photoelectron and $I^-$ fragment should be then determined by the relative speeds of those two distinct processes, opening the new way of the reaction control for the anion chemistry possibly through the control of the quantum-mechanical nature of the DBS resonant doorway. The mode-specific competition dynamics is quite dramatic. For instance, the autodetachment signal of the $10'^1$ mode is much stronger than that of the $11'^1$ mode in the photodetachment spectrum, whereas that of the latter ($11'^1$) is expected to be much stronger compared to that of the former ($10'^1$) as it is supposed to follow the Franck-Condon (FC) principle. On the contrary, the $I^-$ fragment yield at the $11'^1$ mode excitation is found to be much stronger

than that observed at the $10'^1$ mode excitation in the fragment action spectrum, Fig. 1. This conforms with the FC simulation whereas it is exactly opposite to the trend found in the photodetachment spectrum. This should be ascribed to the fact that the autodetachment rate of the $10'^1$ mode is much faster than that of the $11'^1$ mode according to the Fermi's golden rule mainly due to the stronger IR intensity of the former (*vide supra*), giving the relatively larger autodetachment yield of $10'^1$ compared to $11'^1$. That is, the autodetachment process at the $10'^1$ mode excitation should prevail in the competition with the DBS-VBS transition, while it is completely the other way around for the $11'^1$ mode excitation. The photodetachment signal from the DBS of *p*-$IPhO^-$ is dynamically controlled! It should be emphasized that the DBS lifetime estimated from the photoelectron transient (Fig. 2) represents the kinetic sum of all relaxation pathways including the autodetachment and DBS-VBS transition processes, and thus the autodetachment rate alone could not be solely extracted. Therefore, the relative yield of the auto-detached photoelectron compared to the $I^-$ fragment yield, manifested in the respective photodetachment and fragment-action spectra, should reflect the mode-dependent competition dynamics between two major relaxation pathways. It should also be noted that both the autodetachment and the anion fragmentation occur most significantly only at the DBS resonances, indicating that the DBS resonant states play the essential role as the doorway into the anion chemistry. This confirms the long-standing premise that the DBS plays the role of the doorway to the anion formation and subsequent chemical reactions such as DEA.[32]

The situation is somewhat different for the case of *m*-$IPhO^-$. The lifetime of the DBS is quite short ($\tau$ < ~ 2 ps) even at the ZPL (Fig. 2), and thus the photoelectron yield originating from autodetachment is much diminished to give the featureless photodetachment spectrum. Instead, the resonant peak corresponding to the ZPL of DBS has been clearly observed in the $I^-$ fragment action spectrum, Fig. 1. The bandwidth of the DBS band is quite broad, indicating that it might survive only briefly with the time constant less than hundreds of femtoseconds. Although the additional spectral bands attributable to DBS resonances could be further identified, the broad

structureless background signal is dominant in the whole $I^-$ fragment action spectrum. The overall shape of the $I^-$ fragment action spectrum in the wide excitation energy range does not follow that of the photodetachment spectrum (Supplementary Information), suggesting that there may exist the new channel responsible for the $I^-$ fragment regardless of the photodetachment cross section. The broad spectral feature in the $I^-$ action spectrum starts to appear much below the EA threshold, and this could be the consequence from the direct excitation to the repulsive $S_1$ ($\pi\sigma^*$) state of the *m*-$IPhO^-$ anion especially since $S_1$ is predicted to be located much below $D_0$ in the vertical transition region (Fig. 3). The direct anionic $S_1$-$S_0$ excitation leading to the prompt C-I bond cleavage then competes with the direct photodetachment process, while the indirect fragmentation/autodetachment channel mediated by the DBS Feshbach resonances gets relatively less efficient for *m*-$IPhO^-$. The excited-state dynamics of the anion chemistry has been quite rarely investigated because that the cross-section of the direct photodetachment is huge and increases quite rapidly with increasing the energy to overwhelm the whole excitation process. In this regard, the excited-state dynamics of the *m*-$IPhO^-$ anion found here is very unique and subject to the further investigation in the near future.

In summary, the long-time premise that the dipole-bound state plays the dynamic role of the doorway to the anion chemistry and physics has been experimentally demonstrated here. The C-I chemical bond rupture of *ortho*-, *meta*-, or *para*-iodophenoxide anion (giving the $I^-$ fragment) is found to be mediated by the distinct DBS resonances and occurs competitively with the concomitant autodetachment process. For DBS resonant states above EA, the relative yields of the C-I fragmentation and the electron-detachment channels are found to be kinetically controlled, and thus strongly mode-specific to give the great promise for the new way of the anion reaction control by tuning the quantum-mechanical nature of the vibronic excitation. Dynamic behavior at the DBS resonances below EA unravels the mechanism of the DBS-VBS nonadiabatic transitions of three different isomers. For *meta*- or *para*-iodophenoxide, the efficient internal conversion from the metastable DBS into the valence-bound $S_1$ ($\pi\sigma^*$) state (which is repulsive along the C-I bond elongation coordinate) should be responsible for the fast relaxation followed

by the subsequent C-I bond fragmentation. The rate of the nonadiabatic transition of the *ortho*-iodophenoxide anion is however found to be nearly two orders of magnitudes slower than that of *meta*-, or *para*-iodophenoxide, explaining why the C-I bond fragmentation yield of *ortho*-iodophenoxide stands out only at the DBS resonance below the EA threshold. Curve crossings of the potential energy surfaces of DBS and the nearby anionic valence state(s) particularly along the dissociative C-I bond extension coordinate are found to be critical for the conveyance of the electron into or out of the valence orbital. The more sophisticated theoretical calculations would be quite desirable in the coming years.

**Methods**

**Electrospray ionization-photoelectron imaging set-ups.** For sampling, the 1 mM samples of *o*-, *m*-, or *p*-iodophenol (TCI Chemicals Inc.) were dissolved in the 9:1 methanol/water mixed solvent. Each anion was generated by the negative mode of the home-made electrospray ionization (ESI) source by applying the -3000 V emission voltage. Anions were entered into the vacuum chamber through a heated capillary at ~ 180 °C and de-solvated by a dual-stage ion funnel (IF141, Masstech Inc.). Isolated anions were guided into the cryogenically cooled (8 K) Paul ion trap by passing through a series of hexapole, quadrupole, and octopole ion guides. After the trapping time of ~ 50 ms, the internally cooled anions were extracted into the velocity map photoelectron imaging electrodes to be intersected by the picosecond or nanosecond laser pulses. Photoproducts (electron or fragment) generated by the laser pulses were detected by the chevron-type microchannel plates (MCP) backed by the phosphor screen. The photoelectron images were recorded by a charge-coupled device (CCD) camera whereas the photoelectron signals were recorded by the photomultiplier tube (PMT). Photoelectron images were reconstructed by the BASEX or polar onion peeling (POP) program.[60, 61]

**Picosecond/nanosecond pulsed laser set-ups.** Picosecond laser pulses were generated from the Ti:sapphire regenerative amplifier (Legend Elite-P, Coherent) seeded by the femtosecond oscillator (Vitara-T-HP, Coherent). A half of fundamental output was frequency tuned by the

optical parametric amplifier (TOPAS-800, Light Conversion) to be used as the pump laser pulse, while the other half was used for probing. The temporal delay between the pump and probe laser pulses was controlled by using a retro-reflector (UBBR2.5-1UV) placed on a 220 mm-long optical delay stage (DDS220, Thorlabs). A tunable nanosecond laser pulse was generated from a Nd:YAG laser system equipped with multiple harmonic generators (NT342, Ekspla).

**Computational methods.** All calculations were performed by using the density functional theory (DFT) at the B3LYP/def2TZVP level in the Gaussian 09 package. The Franck-Condon simulation of $S_0$-$D_0$ transition was calculated by using the ezSpectrum program[62] based on the calculated harmonic frequencies of $S_0$ and $D_0$ at the optimized geometries.

**Associated Content**

Supporting Information

Details of the DBS vibrational peak assignments, resonant/non-resonant photoelectron spectrums, and other supportive experimental/theoretical data were described.

**Author Information**

Corresponding author

Sang Kyu Kim

*sangkyukim@kaist.ac.kr

ORCID

Do Hyung Kang: 0000-0003-4774-9062

Jinwoo Kim: 0000-0003-2967-6904

Han Jun Eun: 0000-0002-0848-0948

Sang Kyu Kim: 0000-0003-4803-1327

**Conflicts of the interest**

Author declares that there is no competing interest in this article.

**Acknowledgement**

This work was supported by the National Research Foundation of Korea under the Project Numbers of 2019R1A6A1A10073887, and 2018R1A2B3004534.

**References**

1. Fermi, E. & Teller, E. The Capture of Negative Mesotrons in Matter. *Phys. Rev.* **72**, 399-408 (1947).
2. Jordan, K. D. & Wang, F. Theory of Dipole-Bound Anions. *Annu. Rev. Phys. Chem.* **54**, 367-396 (2003).
3. Compton, R. N. & Hammer, N. I. *Multipole-bound Molecular Anion*. In: Babcock, L. M., Adams, N. G. (eds). *Advances in Gas Phase Chemistry*, vol. 4.(Elsevier, 2001).
4. Lykke, K. R., Mead, R. D. & Lineberger, W. C. Observation of Dipole-Bound States of Negative Ions. *Phys. Rev. Lett.* **52**, 2221-2224 (1984).
5. Zhu, G.-Z. & Wang, L.-S. High-resolution photoelectron imaging and resonant photoelectron spectroscopy via noncovalently bound excited states of cryogenically cooled anions. *Chem. Sci.* **10**, 9409-9423 (2019).
6. Kang, D. H., Kim, J., Noh, H.-R. & Kim, S. K. Observation of the ponderomotive effect in non-valence bound states of polyatomic molecular anions. *Nat. Commun.* **12**, 7098 (2021).
7. Bull, J. N., West, C. W. & Verlet, J. R. R. Ultrafast dynamics of formation and autodetachment of a dipole-bound state in an open-shell π-stacked dimer anion. *Chem. Sci.* **7**, 5352-5361 (2016).
8. Yandell, M. A., King, S. B. & Neumark, D. M. Time-Resolved Radiation Chemistry: Photoelectron

Imaging of Transient Negative Ions of Nucleobases. *J. Am. Chem. Soc.* **135**, 2128-2131 (2013).

9. Garrett, W. R. Critical binding of an electron to a non-stationary electric dipole. *Chem. Phys. Lett.* **5**, 393-397 (1970).
10. Qian, C.-H., Zhu, G.-Z. & Wang, L.-S. Probing the Critical Dipole Moment To Support Excited Dipole-Bound States in Valence-Bound Anions. *J. Phys. Chem. Lett.* **10**, 6472-6477 (2019).
11. Garrett, W. R. Critical Binding of an Electron to a Rotationally Excited Dipolar System. *Phys. Rev. A* **3**, 961-972 (1971).
12. Abdoul-Carime, H. & Desfrançois, C. Electrons weakly bound to molecules by dipolar, quadrupolar or polarization forces. *Eur. Phys. J. D* **2**, 149-156 (1998).
13. Gutowski, M., Skurski, P., Boldyrev, A. I., Simons, J. & Jordan, K. D. Contribution of electron correlation to the stability of dipole-bound anionic states. *Phys. Rev. A* **54**, 1906-1909 (1996).
14. Yuan, D.-F., Liu, Y., Qian, C.-H., Zhang, Y.-R., Rubenstein, B. M. & Wang, L.-S. Observation of a π-Type Dipole-Bound State in Molecular Anions. *Phys. Rev. Lett.* **125**, 073003 (2020).
15. Bull, J. N., Anstöter, C. S. & Verlet, J. R. R. Ultrafast valence to non-valence excited state dynamics in a common anionic chromophore. *Nat. Commun.* **10**, 5820 (2019).
16. Bailey, C. G., Dessent, C. E. H., Johnson, M. A. & Bowen, K. H. Vibronic effects in the photon energy-dependent photoelectron spectra of the $CH_3CN^-$ dipole-bound anion. *J. Chem. Phys.* **104**, 6976-6983 (1996).
17. Cao, W., Zhang, H., Yuan, Q., Zhou, X., Kass, S. R. & Wang, X.-B. Observation and Exploitation of Spin–Orbit Excited Dipole-Bound States in Ion–Molecule Clusters. *J. Phys. Chem. Lett.* **12**, 11022-11028 (2021).
18. Sidorkin, V. F., Belogolova, E. F., Doronina, E. P., Liu, G., Ciborowski, S. M. & Bowen, K. H. "Outlaw" Dipole-Bound Anions of Intra-Molecular Complexes. *J. Am. Chem. Soc.* **142**, 2001-2011 (2020).
19. Belogolova, E. F., Liu, G., Doronina, E. P., Ciborowski, S. M., Sidorkin, V. F. & Bowen, K. H. Dipole-Bound Anions of Intramolecular Complexes. *J. Phys. Chem. Lett.* **9**, 1284-1289 (2018).
20. Lu, Y., Tang, R. & Ning, C. Observation of an Excited Dipole-Bound State in a Diatomic Anion. *J. Phys. Chem. Lett.* **12**, 5897-5902 (2021).
21. Gutowski, M., Skurski, P. & Simons, J. Dipole-Bound Anions of Glycine Based on the Zwitterion and Neutral Structures. *J. Am. Chem. Soc.* **122**, 10159-10162 (2000).

22. Ashworth, E. K., Anstöter, C. S., Verlet, J. R. R. & Bull, J. N. Autodetachment dynamics of 2-naphthoxide and implications for astrophysical anion abundance. *Phys. Chem. Chem. Phys.* **23**, 5817-5823 (2021).

23. Laws, B. A., Levey, Z. D., Schmidt, T. W. & Gibson, S. T. Velocity Map Imaging Spectroscopy of the Dipole-Bound State of $CH_2CN^-$: Implications for the Diffuse Interstellar Bands. *J. Am. Chem. Soc.* **143**, 18684-18692 (2021).

24. Bull, J. N. *et al.* Nonadiabatic Dynamics between Valence, Nonvalence, and Continuum Electronic States in a Heteropolycyclic Aromatic Hydrocarbon. *J. Phys. Chem. Lett.* **12**, 11811-11816 (2021).

25. Zhang, Y.-R., Yuan, D.-F. & Wang, L.-S. Observation of Core-Excited Dipole-Bound States. *J. Phys. Chem. Lett.* **13**, 2124-2129 (2022).

26. Wang, H. *et al.* Protein Dynamics Control the Kinetics of Initial Electron Transfer in Photosynthesis. *Science* **316**, 747-750 (2007).

27. Sanche, L. Low energy electron-driven damage in biomolecules. *Eur. Phys. J. D* **35**, 367-390 (2005).

28. Gu, J., Xie, Y. & Schaefer, H. F. Near 0 eV Electrons Attach to Nucleotides. *J. Am. Chem. Soc.* **128**, 1250-1252 (2006).

29. Boudaïffa, B., Cloutier, P., Hunting, D., Huels, M. A. & Sanche, L. Resonant Formation of DNA Strand Breaks by Low-Energy (3 to 20 eV) Electrons. *Science* **287**, 1658-1660 (2000).

30. Lv, X. *et al.* Ultrafast Photoinduced Electron Transfer in Green Fluorescent Protein Bearing a Genetically Encoded Electron Acceptor. *J. Am. Chem. Soc.* **137**, 7270-7273 (2015).

31. Verlet, J. R. R., Anstöter, C. S., Bull, J. N. & Rogers, J. P. Role of Nonvalence States in the Ultrafast Dynamics of Isolated Anions. *J. Phys. Chem. A* **124**, 3507-3519 (2020).

32. Sommerfeld, T. Dipole-bound states as doorways in (dissociative) electron attachment. *J. Phys.: Conf. Ser.* **4**, 245-250 (2005).

33. Tripathi, D. & Dutta, A. K. Electron Attachment to DNA Base Pairs: An Interplay of Dipole- and Valence-Bound States. *J. Phys. Chem. A* **123**, 10131-10138 (2019).

34. Zawadzki, M. *et al.* Resonances and Dissociative Electron Attachment in HNCO. *Phys. Rev. Lett.* **121**, 143402 (2018).

35. Narayanan S J, J., Tripathi, D. & Dutta, A. K. Doorway Mechanism for Electron Attachment Induced DNA Strand Breaks. *J. Phys. Chem. Lett.* **12**, 10380-10387 (2021).

36. Ma, J. *et al.* Observation of dissociative quasi-free electron attachment to nucleoside via excited

anion radical in solution. *Nat. Commun.* **10**, 102 (2019).

37. Pan, X., Cloutier, P., Hunting, D. & Sanche, L. Dissociative Electron Attachment to DNA. *Phys. Rev. Lett.* **90**, 208102 (2003).
38. König, C., Kopyra, J., Bald, I. & Illenberger, E. Dissociative Electron Attachment to Phosphoric Acid Esters: The Direct Mechanism for Single Strand Breaks in DNA. *Phys. Rev. Lett.* **97**, 018105 (2006).
39. Pshenichnyuk, S. A., Modelli, A. & Komolov, A. S. Interconnections between dissociative electron attachment and electron-driven biological processes. *Int. Rev. Phys. Chem.* **37**, 125-170 (2018).
40. Nag, P. & Nandi, D. Fragmentation dynamics in dissociative electron attachment to CO probed by velocity slice imaging. *Phys. Chem. Chem. Phys.* **17**, 7130-7137 (2015).
41. Scheer, A. M., Aflatooni, K., Gallup, G. A. & Burrow, P. D. Bond Breaking and Temporary Anion States in Uracil and Halouracils: Implications for the DNA Bases. *Phys. Rev. Lett.* **92**, 068102 (2004).
42. Martin, F., Burrow, P. D., Cai, Z., Cloutier, P., Hunting, D. & Sanche, L. DNA Strand Breaks Induced by 0-4 eV Electrons: The Role of Shape Resonances. *Phys. Rev. Lett.* **93**, 068101 (2004).
43. Hanel, G. *et al.* Electron Attachment to Uracil: Effective Destruction at Subexcitation Energies. *Phys. Rev. Lett.* **90**, 188104 (2003).
44. Janečková, R., Kubala, D., May, O., Fedor, J. & Allan, M. Experimental Evidence on the Mechanism of Dissociative Electron Attachment to Formic Acid. *Phys. Rev. Lett.* **111**, 213201 (2013).
45. Kunin, A. & Neumark, D. M. Time-resolved radiation chemistry: femtosecond photoelectron spectroscopy of electron attachment and photodissociation dynamics in iodide–nucleobase clusters. *Phys. Chem. Chem. Phys.* **21**, 7239-7255 (2019).
46. Kang, D. H., Kim, J. & Kim, S. K. Recapture of the Nonvalence Excess Electron into the Excited Valence Orbital Leads to the Chemical Bond Cleavage in the Anion. *J. Phys. Chem. Lett.*, 6383-6388 (2021).
47. Kang, D. H., An, S. & Kim, S. K. Real-Time Autodetachment Dynamics of Vibrational Feshbach Resonances in a Dipole-Bound State. *Phys. Rev. Lett.* **125**, 093001 (2020).
48. Kang, D. H., Kim, J. & Kim, S. K. Dynamic role of the correlation effect revealed in the exceptionally slow autodetachment rates of the vibrational Feshbach resonances in the dipole-bound state. *Chem. Sci.* **13**, 2714-2720 (2022).
49. Wang, X.-B. & Wang, L.-S. Development of a low-temperature photoelectron spectroscopy instrument using an electrospray ion source and a cryogenically controlled ion trap. *Rev. Sci.*

*Instrum.* **79**, 073108 (2008).

50. Liu, H.-T., Ning, C.-G., Huang, D.-L. & Wang, L.-S. Vibrational Spectroscopy of the Dehydrogenated Uracil Radical by Autodetachment of Dipole-Bound Excited States of Cold Anions. *Angew. Chem., Int. Ed.* **53**, 2464-2468 (2014).
51. Kim, J. B., Wenthold, P. G. & Lineberger, W. C. Ultraviolet Photoelectron Spectroscopy of o-, m-, and p-Halobenzyl Anions. *J. Phys. Chem. A* **103**, 10833-10841 (1999).
52. Nelson, D. J., Gichuhi, W. K., Miller, E. M., Lehman, J. H. & Lineberger, W. C. Anion photoelectron spectroscopy of deprotonated ortho-, meta-, and para-methylphenol. *J. Chem. Phys.* **146**, 074302 (2017).
53. Nelson, D. J., Gichuhi, W. K., Nichols, C. M., Bierbaum, V. M., Lineberger, W. C. & Lehman, J. H. Photoelectron spectroscopy and thermochemistry of o-, m-, and p-methylenephenoxide anions. *Phys. Chem. Chem. Phys.* **20**, 25203-25216 (2018).
54. Liu, H.-T., Ning, C.-G., Huang, D.-L., Dau, P. D. & Wang, L.-S. Observation of Mode-Specific Vibrational Autodetachment from Dipole-Bound States of Cold Anions. *Angew. Chem., Int. Ed.* **52**, 8976-8979 (2013).
55. Acharya, P. K., Kendall, R. A. & Simons, J. Vibration-induced electron detachment in molecular anions. *J. Am. Chem. Soc.* **106**, 3402-3407 (1984).
56. Simons, J. Propensity rules for vibration-induced electron detachment of anions. *J. Am. Chem. Soc.* **103**, 3971-3976 (1981).
57. Neumark, D. M., Lykke, K. R., Andersen, T. & Lineberger, W. C. Infrared spectrum and autodetachment dynamics of $NH^-$. *J. Chem. Phys.* **83**, 4364-4373 (1985).
58. Yokoyama, K., Leach, G. W., Kim, J. B., Lineberger, W. C., Boldyrev, A. I. & Gutowski, M. Autodetachment spectroscopy and dynamics of vibrationally excited dipole-bound states of $H_2CCC^-$. *J. Chem. Phys.* **105**, 10706-10718 (1996).
59. Anstöter, C. S. *et al.* Mode-Specific Vibrational Autodetachment Following Excitation of Electronic Resonances by Electrons and Photons. *Phys. Rev. Lett.* **124**, 203401 (2020).
60. Roberts, G. M., Nixon, J. L., Lecointre, J., Wrede, E. & Verlet, J. R. R. Toward real-time charged-particle image reconstruction using polar onion-peeling. *Rev. Sci. Instrum.* **80**, 053104 (2009).
61. Dribinski, V., Ossadtchi, A., Mandelshtam, V. A. & Reisler, H. Reconstruction of Abel-transformable images: The Gaussian basis-set expansion Abel transform method. *Rev. Sci. Instrum.*

**73**, 2634-2642 (2002).

62. Gozem, S. & Krylov, A. I. The ezSpectra suite: An easy-to-use toolkit for spectroscopy modeling. *WIREs Computational Molecular Science* **12**, e1546